Treball final de grau

GRAU DE MATEMÀTIQUES

Facultat de Matemàtiques i Informàtica
Universitat de Barcelona

Different dynamical aspects of Lorenz system

Autor: Ainoa Murillo López

Director:	**Dr. Arturo Vieiro Yanes**
Realitzat a:	**Departament de Matemàtiques i Informàtica**
Barcelona,	**27 de juny de 2018**

Abstract

This work is focused on describing the most important properties of the skeleton of the phase space, the Lorenz attractor and the parameter space to understand the Lorenz system. We use different methods to describe the Lorenz system, which includes analytical and numerical tools. Firstly, we summarize some properties and basic concepts of the system, in particular, we study stationary points, bifurcations, invariant manifolds and homoclinic and periodic orbits. Moreover, a description of the geometrical model of the Lorenz attractor is given. Based on this model, we analyse the dynamics of the attractor. We discuss how the strong stable foliation formalizes the numerical evidences obtained previously in different simulations. The existence of this foliation was done through a computer assisted proof, and we also present the main steps of this proof. Finally, this work explores the parameter space using ideas of Kneading theory.

2010 Mathematics Subject Classification. 37C60, 37Dxx

Acknowledgments

I would like to express my most sincere gratitude to Arturo Vieiro, for all his dedication to this project and his comprehension and patience during these months. Thank you for sharing your knowledge with me, without your help this work would not have been possible.

A special thanks to my parents for their support and how they encouraged me to pursue this goal. And specially grateful to my father, who is always by my side to remind me why I chose this path.

And last but not least, thanks to all of those who stood by my side even though I overwhelmed them with this work.

Contents

Dynamical systems are a subject widely studied in different scientific fields, such as engineering, physics, biology, etc. We know from the course Equacions Diferencials that for a two-dimensional dynamical system, defined by a planar vector field, the Poincaré-Bendixson theorem states that every ω-limit set of the orbit of a point, provided the orbit is in a compact set, is either a stationary point, a periodic orbit or a "graphic", that is, a set of stationary points connected by homo/heteroclinic orbits between them. The Poincaré-Bendixson theorem is based on the Jordan Curve Theorem and on properties of the natural ordering of points in $\mathbb{R}$. These ideas cannot be generalized to higher dimensional flows. Indeed, for a three dimensional flow one can have other situations. In this work we shall consider the Lorenz system of equations and we will see that, for suitable parameters, the ω-limit of most of the orbits has a complicated structure.

The Lorenz system is one of the most iconic examples of nonlinear continuous dynamical systems. It was one of the first examples showing up dissipative chaos. Lorenz equations define a simple quadratic polynomial vector field. But the associated dynamics is far from being trivial. It took large effort to understand the mechanism leading to chaos. There is a huge amount of papers, books and material available on the Lorenz system. We have referred a short amount of references only, those that helped in this work or where related data can be obtained.

Following previous ideas of Satzman, E. Lorenz approximated the motion of the atmosphere using a 2-layer model where the fluid (a gas) is contained representing the upper and lower part of the atmosphere. Different constant temperature is considered in the two layers. This creates a external force on the fluid which causes the convection. If the gradient of temperature is large enough the convection becomes turbulent. This is the regime he was interested in. To be able to perform simulations, he reduced the PDE equations to a simple system of 3 differential equations. Although this simplification might be too rough to describe the actual motion of the atmosphere, he investigated the reduced system and show that most orbits have sensitivity with respect to initial conditions, which is an important ingredient for having chaos in the system. Concretely, after several simplifications, E. Lorenz deduced the so-called Lorenz equations in 1963, [9],

$$\begin{cases} \dot{x} = \sigma(y - x), \\ \dot{y} = \rho x - y - xz, \\ \dot{z} = -\beta z + xy, \end{cases}$$

where the parameters σ, β and ρ represent magnitudes describing the atmosphere properties. Concretely, σ is the so-called Prandtl coefficient, ρ refers to the Rayleigh coefficient and β is an scaling (aspect-ratio) coefficient. These are typical quantities to describe the properties of fluids in general.

For the classical parameters $\sigma = 10$, $\beta = 8/3$ and $\rho = 28$, E. Lorenz observed a stable chaotic attractor. However, all his considerations where based on intuitive ideas but far from being rigorous. It took several years to formalize what he observed and prove the existence of the attractor. Several geometrical considerations and analytical approaches

where developed to this end. Furthermore, the last step required a computer assisted proof. This was done by W. Tucker, [14], who proves the existence of the Lorenz attractors using rigorous theoretical concepts and the constructions of a numerical method with precise error estimation.

The goal of this work is to review the geometrical mechanisms that leads to the formation of the Lorenz attractor and to stablish the main features of its structure. To this end, we shall combine theoretical tools with simple numerical illustrations to obtain some insights. The theoretical tools include basics of dynamical systems theory (bifurcations, stability, etc), local analysis and global geometrical tools. For the numerics we have implemented a Taylor method with variable stepsize, see appendix A. Using our implementation we have explore both the phase space and the parameter space of the Lorenz system.

In chapter 1, we summarize some properties of the Lorenz system and basic concepts of dynamical systems. Chapter 2 is devoted to describe the most important characteristics of the phase space as a first step to understand the Lorenz system. In particular, we will provide basic results concerning its stationary points, bifurcations, invariant manifolds and homoclinic and periodic orbits.

In 1979 Guckenheimer and Williams, [6], introduced the geometric Lorenz model and proved that it has a strange attractor. The behaviour showed in numerical simulations of the Lorenz system, seems to satisfy the properties of the geometric Lorenz model. In particular, a flow that satisfies these properties contains a strange attractor, called the geometric Lorenz attractor. This geometric model is described in Chapter 3.

The existence of the Lorenz attractor relies on the existence of a strong stable foliation. We shall review the main ideas behind this assertion. Note that for concrete values of the parameter, for example for classical ones, the existence of the foliation is stablished through a computer assisted proof, [14]. The main steps of this proof will be discussed in Chapter 4.

Finally, Chapter 5 contains a numerical exploration of the parameter space with the goal to stablish parameter regions corresponding to Lorenz attractors with different topological properties.

During the development of this work, the Lorenz system has been studied using several methods that are applicable to any dynamical system. We have combined analytic techniques with numerical integration of the system. The main goal has been to determine the main parts of the skeleton of the system, that organizes the phase space dynamics of a dynamical system.

One of the main methodologies used to describe the topology of the phase space has been the use of a Poincaré map to study the behaviour of the system. We have numerically computed the iterates of Poincaré maps but we also have investigate them from analytical point of view to understand the derivation of suitable return map models. With the same

aim, the Kneading theory has been used to study the parameter space.

To sum up, this work shows important results of the Lorenz system obtained by using different methods that we have studied and particularized for the Lorenz system. Beyond the particular knowledge of Lorenz system, this work has allowed me to extend my knowledge about dynamical systems in general and how to systematically use different techniques to study its dynamics.

Chapter 1

Introduction to Lorenz equations

In this chapter we provide a general view of the Lorenz equations. These are a three-dimensional system of ordinary differential equations, which was derived from a model of fluid convection. They are:

$$\begin{cases} \dot{x} = \sigma(y - x), \\ \dot{y} = \rho x - y - xz, \\ \dot{z} = -\beta z + xy, \end{cases} \tag{1.1}$$

where $(x, y, z) \in \mathbb{R}^3$ and $\sigma, \beta, \rho > 0$, where σ is called the Prandtl coefficient , ρ is the Rayleigh coefficient and β is called the aspect ratio coefficient.

E. D. Lorenz used in [9] $\sigma = 10$, $\beta = \frac{8}{3}$ and $\rho = 28$. A solution of the Lorenz equations for these parameters is shown in Fig. 1.1, where we illustrate the positive semiorbit of an initial condition close to the origin. Concretely, the figure 1.1 shows the positive semiorbit of a chosen initial point which tends to the so-called Lorenz attractor. From the initial point the orbit spirals around one sheet of the attractor and then jump over the other sheet, where it loops until it jumps to the original one and so on. All orbits of different initial points, behaves qualitatively to the same Lorenz attractor even though they do not have the same behaviour. Despite it seems that the Lorenz attractor lies in a 2-dimensional manifold (the union of the two sheets), we will see that this is not true and has a kind of fractal structure.

In this work we are interested in dynamical properties of Lorenz system. The Lorenz equations define a dynamical system. We recall some basic concepts related to dynamical systems theory.

Definition 1.1. Let T be a time set (in $\mathbb{R}$ or $\mathbb{C}$ for continuous time, or in $\mathbb{Z}$ for discrete time). An **evolutionary process** with a phase space, extended to an open set $\Omega \subset T \times \mathbb{R}^n$ and a domain $D \subset T \times \Omega$ is a continuous application

$$\Phi : D \longrightarrow \mathbb{R}^n$$

$$(t; t_0, x_0) \longrightarrow \Phi(t; t_0, x_0)$$

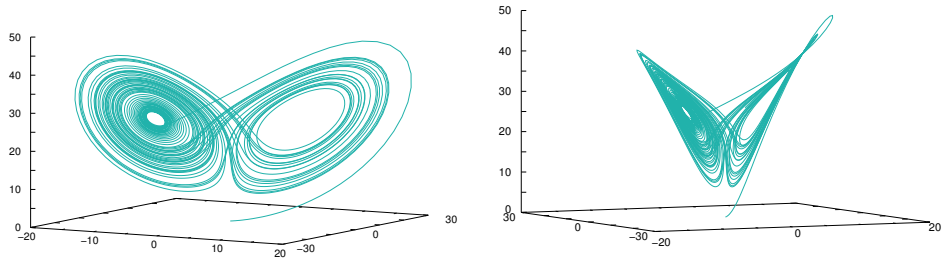

Figure 1.1: Positive semiorbit of the point $(0.1, 0.1, 0.1)$. The orbit tends to a complicated structure called the Lorenz attractor. Left: We see that the orbit spirals in one part of the attractor and eventually jumps to the other part. Right: We see that the two parts are thin and the orbit seems to lie in a planar surface.

such that for all $(t_0, x_0) \in \Omega$, $t_1 \in T$:

1. $t_0 \in T$ and $\Phi(t_0; t_0, x_0) = x_0$.
2. If $t_0, t_1, t_2 \in T$, then $\Phi(t_2; t_1, \Phi(t_1; t_0, x_0)) = \Phi(t_2; t_0, x_0)$.

When an evolutionary process is associated to an ordinary differential equation $\dot{x} = F(t, x)$, under suitable regularity conditions of F, one has that Φ verifies:

3. D is an open set and, for all $(t_0, x_0) \in \Omega$, $I(t_0, x_0) = \{t \in \mathbb{R} | (t; t_0, x_0) \in D\}$ is an open interval. Here $I(t_0, x_0)$ is the maximal interval of the solution of Cauchy problem starting for t_0 and x_0.
4. Φ is derivative respect t, and the partial derivative $\frac{\partial \Phi}{\partial t} : D \longrightarrow \mathbb{R}^n$ is continuous.

Definition 1.2. A **dynamical system** is a tuple (T, M, Φ_t), where T is as above, M is a non-empty manifold (the so-called phase space) and $\Phi_t = \Phi(t; t_0, x_0)$ is an evolution operator satisfying the uniparametric group properties 1. and 2. above.

Dynamical system with $T = \mathbb{R}$ are associated to ordinary differential equations, while dynamical system with discrete time are associated to diffeomorphisms. In this work will appear both continuous dynamical systems and discrete dynamical systems, which will be obtained from continuous systems by the Poincaré map.
Note that in definition 1.1 we have consider that we can evaluate evolutionary processes for all t. In our case, we have a dynamical system given by the ordinary differential equations 1.1.
If M is a compact manifold, then the flow is defined for all t. However the Lorenz system is defined in $\mathbb{R}^3$ so in general, the flow could not be defined for all t.

We will see in section 1.2 that Lorenz equations are defined for all $t \in \mathbb{R}$. In particular the attractor is in a compact set, so in this case we will treat a dynamical system in a compact set. Besides the Lorenz system contains a global attractor, in this chapter are given some global properties of the flow associated to the Lorenz system.

Usually one studies the phase space of a dynamical system starting with the skeleton, formed by stationary points, periodic orbits, invariant sets and its homoclinic and heteroclinic connections.

Definition 1.3. We define an **invariant set** S for a flow ϕ_t as a subset $S \subset \mathbb{R}^n$ such that

$$\phi_t \in S \text{ for } x \in S \text{ for all } t \in \mathbb{R}.$$

Definition 1.4. The ω**-limit set** of a point $x \in \mathbb{R}^n$ for ϕ_t is the set of accumulation points of $\phi_t(x)$, when one considers $t \longrightarrow \infty$.
The α**-limit set** of x for ϕ_t is the set of accumulation points of ϕ_t, $t \longrightarrow -\infty$.

We recall that if the orbit of x is bounded then the α and ω-limit sets are non-empty, compact and connected invariant sets. In particular, if $y = \phi_t(x)$ then $\omega(x) = \omega(y)$ and $\alpha(x) = \alpha(y)$. One speaks about α, ω-limit of orbits.

Definition 1.5. A **homoclinic orbit** to an invariant object x_* is a non-trivial orbit with α and ω-limit equal to x_*. A **heteroclinic orbit** (between two invariant objects x_* and y_*) is a orbit which tends towards x_* in reverse time and towards y_* in forwards time.

We first note that the Lorenz system has a symmetry $L(x, y, z) = (-x, -y, z)$ for all values of the parameters β, σ, and ρ. That is, the solutions are symmetrical with respect to the z-axis. This follows from the following simple observation. If $(x(t), y(t), z(t))$ is a solution then $(-x(t), -y(t), z(t))$ is also a solution of the equations because

$$(-x)' = -\sigma(y - x) = \sigma((-y) - (-x)), \qquad (-y)' = -x(\rho - z) + y = (-x)(\rho - z) - (-y).$$

Indeed the z-axis, $x = y = 0$, is invariant. The restricted dynamics to $x = y = 0$ is $\dot{z} = -\beta z$. Hence, for $\beta > 0$, the origin is a fixed point of the system and the z-axis is an attracting direction. That is, the z-axis is contained on the stable manifold of the origin for all values of the parameters that we consider.

We shall see that the origin has a stable invariant manifold of dimension, at least, two (it depends on ρ, it is 2-dimensional for $\rho > 1$ while for $\rho < 1$ the origin is an attracting node and, hence, it has a 3-dimensional invariant manifold). Here we just note that all the trajectories that starts on the z-axis, remain on it and tends to the origin.
In particular, for $\rho = 1$, the Lorenz system suffers a qualitative change of the topology of the phase space. This variation is what it is called a **bifurcation**. The Lorenz equations presents some bifurcations as a result of changing parameters ρ, σ and β.

1.1 Bifurcations

It is useful to divide bifurcations into two principal classes: local and global bifurcations.

Local bifurcations are those which changes can be entirely analysed considering an arbitrarily small neighbourhood of the stationary point (or the periodic orbit or, in general, of the invariant set considered). Therefore, a local bifurcation can be studied using a Taylor approximation of the system around the invariant set.

In section 2.1 we will try to describe how the Lorenz attractor is created. To this end we shall study the evolution of phase space with respect to parameters. The changes of topology are related to bifurcations. In particular the following local bifurcations will be of interest.

1. **Pitchfork**: Is a local bifurcation where the system transitions from one stationary point to three stationary points. Pitchfork bifurcation is generic to problems that have symmetry. One usually requires to have a line of stationary points for all values of λ.

   A Pitchfork bifurcation is called supercritical if the new stationary point exists for values greater than the bifurcation value. Otherwise, the Pitchfork bifurcation is called subcritical. As a simple model to illustrate a supercritical Pitchfork bifurcation (which occurs for the Lorenz system for $\rho = 1$), we consider

   $$\dot{x} = \mu x - x^3. \tag{1.2}$$

   For $\mu < 0$, there is one stable stationary point at $x = 0$. For $\mu > 0$, the origin is an unstable stationary point and there is two stable stationary points at $x = \pm\sqrt{\mu}$. This situations is analogous for the Lorenz system.

2. **Hopf**: Is a local bifurcation in which a equilibrium point of focus type changes the stability and, as a by product, a periodic orbit can be created/destroyed. A Hopf bifurcation occurs when a pair of complex conjugate eigenvalues cross the imaginary axis of the complex plane.

   A Hopf bifurcation is called supercritical if a stable limit cycle surrounds an unstable focus equilibrium point. Otherwise, if an unstable limit cycle surrounds a stable focus point then the Hopf bifurcation is referred as subcritical. We are interested in the subcritical case since, for the Lorenz system, a subcritical Hopf bifurcation happens for $\rho = \rho_h = 470/16 \approx 24.76$. As a simple model to illustrate this type of bifurcations we consider the following planar system

   $$\dot{r} = r(r^2 + \mu), \qquad \dot{\theta} = 1,$$

   which is expressed in polar coordinates (r, θ). For $\mu < 0$, the origin is an stable focus and there is an unstable limit cycle. This cycle collides with the origin when $\mu = 0$ and disappears for $\mu > 0$ when the origin becomes an unstable focus. The situation

is analogous for the Lorenz system.

Global bifurcations are those which are not local, that is if they cannot be analysed in a small neighbourhood of the invariant object. There is not a systematic way to study global bifurcations. Some of them are associated to global changes on the topology of the phase space, caused by homoclinic or heteroclinic explosions between invariant objects.

In the Lorenz system we can observe some global bifurcations, as for example T-points, see section 5.2. We will not do a deep study of all of them. However, we will see in Section 2.3 that a global bifurcation plays a key role in the formation of the Lorenz attractor. In such a bifurcation a limit cycle is born from a homoclinic connection.

1.2 Global attractor

To study a dynamical system, usually we analyse the behaviour of the solutions. In particular for the Lorenz system this requires some previous concepts to define the Lorenz attractor. In the following we assume that a vector field $\dot{x} = F(x)$, $x \in \mathbb{R}^n$, $F \in C^1(\mathbb{R}^n)$ is given, and we denote by ϕ_t the associated flow.

Definition 1.6. The closed invariant set Λ is **indecomposable** if for every pair of points x, y in Λ and $\varepsilon > 0$, there are $x = x_0, x_1, \cdots, x_{n-1}, x_n = y$ and $t_1, \cdots, t_n \geq 1$ such that the distance from $\phi_t(x_{i-1})$ to x_i is smaller than ε.

Definition 1.7. An **attractor** is an indecomposable closed invariant set Λ with the property that, given $\varepsilon > 0$, there is a set U of positive Lebesgue measure in the ε-neighbourhood of Λ such that $x \in U$ implies that the ω-limit set of x is contained in Λ, and the forward orbit of x is contained in U. We shall call an attractor **strange** if it contains a transversal homoclinic orbit.

In fact, the Lorenz system contains a global attractor. This follows from the existence of a trapping region which contains the Lorenz attractor. Thus the orbits do not diverge to infinity and the system has global stability. To prove this fact we use the following function:

$$V = \frac{1}{2}(x^2 + y^2 + (z - \sigma - \rho)^2).$$

Note that

1. $V : R^3 \longrightarrow \mathbb{R}$ is differentiable with respect to all the variables,
2. $V \geq 0$ for all $(x, y, z) \in \mathbb{R}^3$,
3. $\frac{dV}{dt}(x(t), y(t), z(t)) = xx' + yy' + (z - \sigma - \rho)z' = -\sigma x^2 - y^2 - \beta z^2 + \beta(\sigma + \rho)z$, where $(x(t), y(t), z(t))$ is a solution of the Lorenz equations.

Let $S := \{(x, y, z) \in \mathbb{R}^3 : \frac{dV(x,y,z)}{dt} \geq 0\}$ be a bounded region and let

$$E := \{(x, y, z) \in \mathbb{R}^3 : \sigma x^2 + y^2 + \beta z^2 = \beta(\sigma + \rho)z\} \subset S,$$

be a bounded ellipsoid. Then

$$x \notin S \implies \frac{dV(x)}{dt} < 0.$$

In fact, $\frac{dV(x)}{dt} \leq -\delta$ for some small $\delta > 0$.

Therefore V decreases strictly until $(x(t), y(t), z(t))$ goes into S with initial conditions $(x(0), y(0), z(0)) = (x, y, z)$.
As S is a non-empty, bounded and positive invariant set, every orbit that moves into S will remain there as the system evolves. Thus S is a trapping region. Therefore the Lorenz flow is defined for all t.

Chapter 2

Phase space structure

In this chapter is given a general view of the phase space structure of the Lorenz system. As varying the value of the parameter ρ, the character of the stationary points and some bifurcations are studied.
The sequence of bifurcations detailed in this chapter leads to the topological structure of the Lorenz attractor.

2.1 Stationary points and bifurcations

Given $\dot{x} = F(x)$ with $x \in \mathbb{R}^n$, x_* is a stationary point if $F(x_*) = 0$. Taking the Lorenz equations we get the following stationary points:

$$\begin{cases} \dot{x} = \sigma(y - x) = 0 \\ \dot{y} = \rho x - y - xz = 0 \\ \dot{z} = -\beta z + xy = 0 \end{cases} \iff \begin{cases} x = y \\ x(\rho - 1 - z) = 0 \\ x^2 = \beta z \end{cases}$$

- If $x = 0$ then $(0, 0, 0)$ is a stationary point.
- If $z = \rho - 1, x = y = \pm\sqrt{\beta(\rho - 1)}$ which implies that
  $C_{1,2} = (\pm\sqrt{\beta(\rho - 1)}, \pm\sqrt{\beta(\rho - 1)}, \rho - 1)$ are stationary points (for $\rho > 1$).

Note that the origin is a stationary point for all values of σ, β and ρ. However, $C_{1,2}$ only exists for $\rho > 1$.

We will study now the character of the stationary points for different values of the parameter ρ. If the stationary point x_* is hyperbolic, using Hartman-Grobman theorem we can study the stability of x_* looking at its linear stability, given by the eigenvalues of the matrix

$$DF(x_*) = \begin{pmatrix} -\sigma & \sigma & 0 \\ \rho - z & -1 & -x \\ y & x & -\beta \end{pmatrix}.$$

We recall that x_* is a hyperbolic point whenever $\mathrm{Re}(\lambda) \neq 0$ for all λ in the spectrum of $DF(x_*)$.

- For $0 < \rho < 1$, the matrix $DF((0,0,0))$ has eigenvalues $\lambda_1 = -\beta$ and $\lambda_{2,3} = \frac{-\sigma-1\pm\sqrt{\sigma^2+(4\rho-2)\sigma+1}}{2}$. One has $\mathrm{Re}(\lambda_i) < 0, i = 1,2,3$, which implies that $(0,0,0)$ is a stable stationary point. The previous reasoning implies local stability, but one has indeed that the origin is global attractor.

  Consider the Lyapunov function (see def. B.1) $V(x,y,z) = \frac{x^2}{\sigma} + y^2 + z^2 \geq 0$, then

  $$\frac{dV}{dt}(x(t),y(t),z(t)) = \frac{2x\dot{x}}{\sigma} + 2y\dot{y} + 2z\dot{z} = 2((\rho+1)xy - x^2 - y^2 - \beta z^2) =$$

  $$= -2\left(x - \frac{\rho+1}{2}y\right)^2 - 2\left(1 - \left(\frac{\rho+1}{2}\right)y\right)y^2 - 2\beta z^2.$$

  As $0 < \rho < 1$, $1 - \left(\frac{\rho+1}{2}\right) > 0$ and therefore $\frac{dV}{dt}(x(t),y(t),z(t)) < 0$.

  So the Lyapunov function is strictly decreasing for all values $(x(t),y(t),z(t))$. Therefore $V(t)$ tend to 0 as t tend to infinity, so $(x(t),y(t),z(t))$ tend to the origin. Thus the origin is a global attractor.

- At $\rho = 1$, one of the eigenvalues of $DF(x_*)$ is equal to 0. In this case we are going to see that a supercritical Pitchfork bifurcation occurs, see left Fig. 2.1.

  Considering the Lorenz equations for $\rho = 1$, we have seen that $DF(x_*)$ has eigenvalues $\lambda_1 = -\beta$, $\lambda_2 = 0$ and $\lambda_3 = -\sigma - 1$. The eigenvectors are $v_1 = (0,0,1)$, $v_2 = (1,1,0)$ and $v_3 = (\sigma,-1,0)$ respectively. As $\lambda_2 = 0$ the Lorenz system has a central manifold, see [5]. To study the dynamics in the $(1,1,0)$ direction, near to $\rho = 1$, consider

  $$\begin{cases} \dot{x} = \sigma(y-x), \\ \dot{y} = \rho x - y - xz, \\ \dot{z} = -\beta z + xy, \\ \dot{\rho} = 0. \end{cases}$$

  which has a 2-dimensional central manifold W^c. We introduce a new parameter $\eta = \rho - 1 \approx 0$ to study the dynamics around the origin, so the system is now

  $$\begin{cases} \dot{x} = \sigma(y-x), \\ \dot{y} = \eta x + x - y - xz, \\ \dot{z} = -\beta z + xy, \\ \dot{\eta} = 0. \end{cases}$$

  The Center Manifold Theorem states that W^c can be locally represented as a graph

  $$\begin{cases} y = g_1(x,\eta) = a_{10}x + a_{01}\eta + a_{20}x^2 + a_{11}x\eta + a_{02}\eta^2 + O(3), \\ z = g_2(x,\eta) = b_{10}x + b_{01}\eta + b_{20}x^2 + b_{11}x\eta + b_{02}\eta^2 + O(3). \end{cases}$$

  Setting this graph to be invariant, we will find the coefficients a_{ij} and b_{ij} and thus we get

  $$\begin{cases} y = x + \frac{1}{\sigma+1}x\eta - \frac{1}{\beta(\sigma+1)}x^3 - \frac{\sigma}{(\sigma+1)^3}x\eta^2 + O(4), \\ z = \frac{1}{\beta}x^2 + \frac{2\sigma}{(\sigma+1)\beta}x^2\eta + O(4). \end{cases}$$

Therefore the dynamics on W^c is

$$\begin{cases} \dot{x} = \sigma(y-x) = \sigma(\frac{1}{\sigma+1}x\eta - \frac{1}{\beta(\sigma+1)}x^3 - \frac{\sigma}{(\sigma+1)^3}x\eta^2) + O(4), \\ \dot{\eta} = 0. \end{cases}$$

Given η, then

$$\dot{x} = \left(\frac{\sigma}{\sigma+1}\eta - \frac{\sigma^2}{(\sigma+1)^3}\eta^2\right)x - \frac{1}{\beta(\sigma+1)}x^3 + O(4).$$

Removing order four terms and scaling time, we obtain:

$$\dot{x} = \left(\beta\sigma\eta - \frac{\sigma^2\beta}{(\sigma+1)^2}\eta^2\right)x - x^3 = \mu x - x^3.$$

In particular one has μ positive for η sufficiently small and that gives a Pitchfork bifurcation, comparing with example 1.2.

The previous computations are analogous to the ones done in [5], but note that there the authors adapt coordinates to the eigenvectors before representing the manifolds as graphs.

- For $\rho > 1$, the origin is unstable. The matrix $DF((0,0,0))$, has three real eigenvalues: $\lambda_1 = -\beta, \lambda_{2,3} = \frac{-\sigma-1\pm\sqrt{\sigma^2+(4\rho-2)\sigma+1}}{2}$.

  λ_2 is positive and, λ_1 and λ_3 are negative, so the origin is a saddle point. Note that $-\lambda_1 < \lambda_2 < -\lambda_3$.

The stable manifold theorem (see [5]) states that if all eigenvalues of $DF(x_*)$ have real part different from zero, then there exists W^s stable manifold, and W^u unstable manifold, such that its tangent spaces have the same dimensions as the stable space E^s, and as the unstable space E^u respectively, generated by the eigenvectors of $DF(x_*)$. Moreover W^s and W^u are tangent to E^s and E^u at x_*. Therefore, the origin has a one-dimensional unstable manifold and a two-dimensional stable manifold.

Recall that in general the stable manifold W^s (respectively, unstable manifold W^u) of a compact invariant set S is the set of points $x \in \mathbb{R}^3$, such that the trajectories through x tend towards S (respectively, towards S in reverse time). By Hartman-Grobman theorem, the local dynamics around x_* is topologically conjugated to the dynamics of the linearized system $\dot{\xi} = DF(x_*)\xi$.

The eigenvalues of $DF(C_{1,2})$ are the roots of the characteristic polynomial

$$P(\lambda) = \lambda^3 + \lambda^2(\sigma+\beta+1) + \lambda\beta(\sigma+\rho) + 2\sigma\beta(\rho-1) = 0.$$

Since σ, β and ρ are positive parameters,

$$P'(\lambda) = 3\lambda^2 + 2\lambda(\sigma + \beta + 1) + \beta(\sigma + \rho) > 0 \qquad \forall \lambda \geq 0.$$

For $\lambda = 0$ we have $P(0) > 0$, and since it is a third degree polynomial equation and its cubic coefficient is positive, we can conclude that all the roots are negative, and at least one of them is real. We denote by $\lambda_1 < 0$ this real eigenvalue.

For the other two roots, denoted $\lambda_{2,3}$ they can be both real or a complex conjugate pair $\lambda_{2,3} = \alpha \pm i\gamma$. Numerically one checks that for $\rho > \rho_c$ ($\rho_c \approx 1.3456$), the roots of $P(\lambda)$ have $\gamma \neq 0$. Summarizing one has:

- For $0 < \rho < \rho_c$, all three eigenvalues are real, so $C_{1,2}$ are saddle points.
- For $\rho > \rho_c$, we have one real eigenvalue and a pair of complex eigenvalues. In this case, $C_{1,2}$ are stationary points of node-focus type.

  Then to study the stability of $C_{1,2}$, we have to consider the $\mathrm{Re}(\lambda_{2,3})$:

  - For $\alpha < 0$, all three eigenvalues have a negative real part, so $C_{1,2}$ are stable focus.
  - For $\alpha > 0$, $C_{1,2}$ are saddle points. Again, by the stable manifold theorem $C_{1,2}$ have a one-dimensional stable manifold and a two-dimensional unstable manifold,
  - At $\alpha = 0$, we have a stability boundary, so we will study for which values of ρ, that occurs.

$$\begin{aligned} P(i\gamma) &= (i\gamma)^3 + (i\gamma)^2(\sigma + \beta + 1) + (i\gamma)\beta(\sigma + \rho) + 2\sigma\beta(\rho - 1) = \\ &= (2\beta\sigma(\rho - 1) - (\beta + \sigma + 1)\gamma^2) + i(\beta(\sigma + \rho) - \gamma^2)\gamma = 0. \end{aligned}$$

  Solving the equations,

$$\begin{cases} 2\beta\sigma(\rho - 1) - (\beta + \sigma + 1)\gamma^2 = 0 \\ \beta(\sigma + \rho) - \gamma^2 = 0 \end{cases} \implies \rho_h = \frac{\sigma(\sigma + \beta + 3)}{\sigma - \beta - 1}.$$

  Let $\sigma = 10$ and $\beta = \frac{8}{3}$, then, $\rho_h = \frac{\sigma(\sigma+\beta+3)}{\sigma-\beta-1} = \frac{470}{19} \approx 24.7468$. Then we have the following:

  * For $\rho < \rho_h$, $C_{1,2}$ are stable. All three eigenvalues of $DF(C_{1,2})$, have negative real part.
  * Consider $\rho = \rho_h$. Here the eigenvalues of $DF(C_{1,2})$ are

$$\lambda_1 = -(\sigma + \beta + 1), \qquad \lambda_{2,3} = \pm i\sqrt{\frac{2\sigma(\sigma + 1)}{\sigma - \beta - 1}}.$$

As $\alpha = 0$, one can numerically observe that ρ_h is the value for which the pair of complex conjugate eigenvalues cross the imaginary axis. Therefore a Hopf bifurcation occurs at the stationary points $C_{1,2}$. Indeed a subcritical bifurcation takes place. As it is been announced in section 1.1, this subcritical Hopf bifurcation destroyed a periodic orbit that arise from a homoclinic orbit. More details about this will be done in section 2.3.

* For $\rho > \rho_h$, $C_{1,2}$ are unstable. $DF(C_{1,2})$ has one negative real eigenvalue and a complex conjugate pair of eigenvalues with positive real part.

2.2 Invariant manifolds

We have seen that for $\rho > 1$, the origin has a one-dimensional unstable manifold and a two-dimensional stable manifold, also called the Lorenz manifold.
In this section we will display the unstable invariant manifold for different values of ρ. Also we will provide some comments on how the stable manifold could be approximated.

The existence of this manifold is given by the stable manifold theorem. So the unstable manifold comes from the eigenvalue $\lambda_2 = \frac{-\sigma-1+\sqrt{\sigma^2+(4\rho-2)\sigma+1}}{2}$.
The corresponding eigenvector of λ_2 is $v_2 = \left(\frac{1-\sigma+\sqrt{\sigma^2+(4\rho-2)\sigma+1}}{2\rho}, 1, 0\right)$.

As these points corresponds to the linear approximation of the unstable manifold, if we take a value in this axis close to the origin we can claim that this point will be in the unstable invariant manifold of $(0,0,0)$. Thus we take as a initial condition the point $(x_0, y_0, z_0) = \frac{v_2}{||v_2||} \cdot 10^{-4}$, and we plot in Fig. 2.1 its orbit using the Taylor method for different values of ρ.

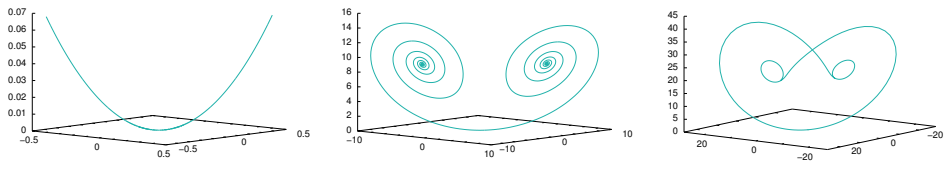

Figure 2.1: We display the one-dimensional invariant manifold of the Lorenz system. From left to right $\rho = 1.2$, 10 and 24.0579.

The Lorenz 2-dimensional manifold can be computed using the parametrization method for invariant manifolds, which is explained with details in [7]. Note that this manifold is extremely difficult to be computed accurately due to the different time-scales (the two stable eigenvalues are of very different magnitude for the parameters we are interested).

In the following we denote by $\dot{x} = F(x)$ the Lorenz system of equations. The invariant stable manifold of $x_* = (0,0,0)$ is denoted by W^s. Let V^L be a 2-dimensional subspace invariant for $\dot{v} = DF(x_*)v$. The aim is to find the 2-dimensional invariant manifold tangent to V^L in x_*, which is the Lorenz manifold. This leads to the so-called "invariance equation". The internal dynamics on W^s is conjugated to the linear dynamics that the linearized equations at x_* have on the linear 2-dimensional stable manifold. This is because the fixed point is a saddle (in particular, hyperbolic).

More concretely, we look for a function W such that $(x,y,z) = W(s_1,s_2)$, with $W(0,0) = x_*$. We require the internal dynamics to be given by $\dot{s} = f(s) = (\lambda_1 s_1, \lambda_3 s_2)$, where $s = (s_1,s_2)$. Thus we get the following Invariance Equation:

$$F(W(s)) = DW(s)f(s). \tag{2.1}$$

Then we consider the Taylor expansion of W,

$$W(s) = \sum_{k\geq 1} W_k(s),$$

where W_k are homogeneous polynomials of degree k. The basic idea is to truncate the series representation to a suitable order so that one obtains a good representation of the local invariant manifold.

To solve the Invariance Equation 2.1 one can use an iterative procedure. The values of $W_1(s)$ are already known (they are the components of the eigenvectors associated to the linearized system at the origin, normalized in a suitable way). For each $k \geq 2$, the goal is to compute $W_k(s)$ assuming that we have already computed $W_i(s)$ for all $i < k$.

Following this method we give the second order approximation of $W(s)$, that is, we solve the invariance equation up to $k = 2$. For concreteness we consider the classical parameters $\sigma = 10$, $\beta = 8/3$ and $\rho = 28$. Since $W(0,0) = (0,0,0)$ the Taylor expansion of second order is given by

$$W(s_1,s_2) = (x(s1,s2), y(s1,s2), z(s1,s2)), \tag{2.2}$$

where

$$\begin{aligned} x(s1,s2) &= a_{10}s_1 + a_{01}s_2 + a_{11}s_1s_2 + a_{20}s_1^2 + a_{02}s_2^2 + O(3),\\ y(s1,s2) &= b_{10}s_1 + b_{01}s_2 + b_{11}s_1s_2 + b_{20}s_1^2 + b_{02}s_2^2 + O(3),\\ z(s1,s2) &= c_{10}s_1 + c_{01}s_2 + c_{11}s_1s_2 + c_{20}s_1^2 + c_{02}s_2^2 + O(3). \end{aligned}$$

The coefficients a_{10}, a_{01}, b_{10}, b_{01}, c_{10} and c_{01} are already known since the values of W_1 can be considered to be the components of the normalized eigenvectors associated to the linearized system at the origin. That is, $a_{10} \approx -0.6148, a_{01} = 0$, $b_{10} \approx 0.7886, b_{01} = 0$, $c_{10} = 0$ and $c_{01} = 1$. Applying the Invariance Equation 2.1, we can compute the coefficients a_{20}, a_{02}, a_{11}, b_{20}, b_{02}, b_{11} and c_{20}, c_{02}, c_{11}. The computations reduce to solve some linear systems. For example, by substituting 2.2 into the invariance equation and collecting terms in s_1^2, we are reduced to solve the linear system $Ax = b$, where $A = DF(0,0,0) - 2\lambda_3 I$ and $b = (0,0,a_{10}b_{10})$. Similar systems are obtained when collecting terms in s_1s_2 and s_2^2.Thus

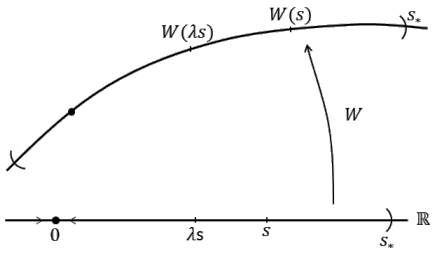

Figure 2.2: Idea of the parametrization $W(s)$ of a one-dimensional stable invariant manifold.

we get

$$W(s_1, s_2) = (-0.6148s_1 + 0.0617s_1s_2, 0.7886s_1 - 0.0957s_1s_2, s_2 + 0.0112s_1^2) + \mathcal{O}(3).$$

Assume that the Taylor series of $W(s)$ has been computed up to a given order. One can determine the maximum value of $\|s\|$, such that the Invariance Equation is satisfied for a given error. This determines a fundamental domain (of radius s_*), where the manifolds are accurately represented by the series. One can see in Fig. 2.2 a sketch for a one-dimensional manifold, with a fundamental interval $(-s_*, s_*)$. In the case of the two-dimensional manifold W, the fundamental domain is a disk.

After determining a fundamental domain where the approximation given by the truncation of the Taylor expansion is accurate, the manifold is globalized from this fundamental domain following an strategy based on numerical integration backward in time that allows to recover the shape of the Lorenz manifold. Details can be found in [7].

2.3 Homoclinic orbit and periodic orbits

An analytic proof of the existence of the homoclinic orbit was done by C. Sparrow in [13]. As this proof is not object of this work, all the arguments done in this section will be based on the behaviour of the orbits.
The heuristic justification given below based on the behaviour of the orbits for different values of the parameter ρ leads to the existence of the homoclinic orbit and the periodic orbits because of the strong stable foliation (see Chapter 4). This is true even though the Lorenz attractor is not contained in a 2-dimensional manifold as its Hausdorff dimension denotes (its Hausdorff dimension is approximately equal to 2.06, [11]).

We have seen that for $\rho > 1$, there's a two-dimensional stable manifold of the origin $W^s((0,0,0))$, see section 2.2. This stable manifold divides $\mathbb{R}^3$ in two sides. For ρ values close to 1, the trajectories that starts at one side tend to C_1, and the ones that starts at the other side tend to C_2. The trajectories that starts at the stable manifold of the origin tend to the origin.

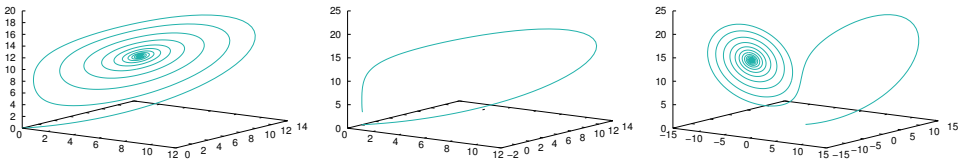

Figure 2.3: From left to right we display the right branch of the one dimensional invariant manifold for $\rho = 13, 13.926$ and 15. The centre plot corresponds (roughly) to the value for which the homoclinic connexion is expected. Accordingly in the left plot, the invariant manifolds spirals around C_1 and in the right plot it spirals around C_2. By symmetry the left branch does the same.

For a value of the parameter ρ ($\rho' \approx 13.926$), there's a change on the behaviour of the orbits. For $\rho < \rho'$, the spirals formed by the trajectory that starts at the unstable manifold of the origin grow larger and larger around C_1 or C_2 respectively (Fig. 2.3 Left). For $\rho > \rho'$, the trajectories cross and they are attracted by the other stationary point (Fig. 2.3 Right). For $\rho = \rho'$, the trajectories that starts at the unstable manifold of the origin, tend to the stable manifold of the origin, so they tend for backward and forward time to the origin. Therefore there's an homoclinic orbit associated to the stationary point $(0, 0, 0)$ (Fig. 2.3 Center). At this parameter a limit cycle is born through a mechanism that we represent, for a planar vector field, in Fig. 2.4. This is a consequence of the Poincaré-Bendixson theorem. The same situation happens for the Lorenz system, see section 2.1.

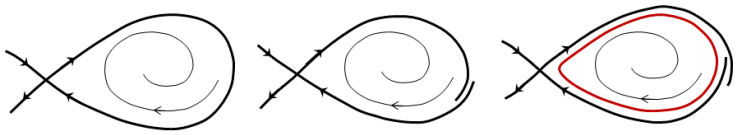

Figure 2.4: Sketch of the birth of an repelling limit cycle from a homoclinic loop to a saddle stationary point.

Now we will study periodic orbits for $\rho > \rho'$. There exist different techniques to compute numerically approximations of the periodic orbits but to use these techniques, a good approximation of the position and the period of an orbit is needed.
As the value of ρ decreases towards ρ', the period of the orbit increases and gets closer to the origin. This fact suggests that the orbit comes from the homoclinic explosion at ρ'.
For values of $\rho < \rho_h$ the period of the orbit is quite small. We have seen that for $\rho = \rho_h$ a subcritical Hopf bifurcation occurs, then, as ρ approaches to that value, the periodic orbit gets smaller and it tends to a stationary point.

Chapter 3

Geometric model

After seeing some properties of the Lorenz equations, and some numerical results, J. Guckenheimer and R. F. Williams introduced in [6] the so-called geometric Lorenz attractor, as a model to explain the behaviour of the solutions of the Lorenz equations. The hardest part of those results is to check that the geometric model indeed corresponds to the Lorenz attractor. This was done by W. Tucker in the computer assisted proof. The main ideas of Tucker's approach will be discussed in the following chapter.

3.1 The derivation of the model differential equations

The geometric Lorenz model is a return map model. The return map is obtained as the composition of two maps. One of the map describes the local dynamics near the saddle at $(0,0,0)$. This local passage can be approximated by the linear flow. The second map is a global map that reinjects the dynamics. See Fig. 3.1 for a sketch of the construction of the return map, the two maps are indicate by the red and the blue arrows, respectively.
First, we derive the local map using the linearized system around the origin. As $(0,0,0)$ is a hyperbolic singularity, the Lorenz system is, locally, topologically equivalent to the linearized system around $(0,0,0)$. We will construct a topological 3-cell T, described in terms of linear differential equations:

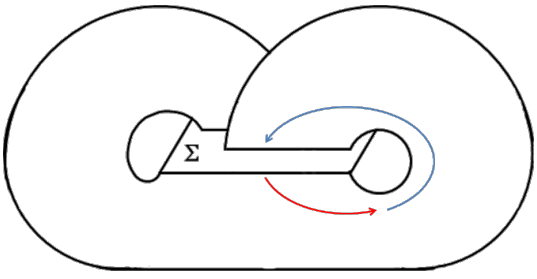

Figure 3.1: Sketch of the maps involved in the geometric Lorenz model.

$$\begin{cases} \dot{x} = \lambda_2 x, \\ \dot{y} = \lambda_3 y, \\ \dot{z} = \lambda_1 z, \end{cases} \quad \text{where we assume } 0 < -\lambda_1 < \lambda_2 < -\lambda_3.$$

Let $\Sigma = \{(x, y, 1) : |x| \leq 1/2, |y| \leq 1/2\}$. Σ will be considered to be the top square of the 3-cell T. Assume that Σ is a transverse section to the flow, so that every trajectory eventually crosses Σ. Σ is what we call a Poincaré section. In particular, there is an open set $U \in \mathbb{R}^3$, with $(x_0, y_0, z0) \in \Sigma$ such that for all $(x, y, z) \in U$, there exists a $\tau(x, y, z)$ such that $\varphi(\tau(x, y, z), (x, y, z)) \in \Sigma$.

Solving this linear system with initial conditions $(x_0, y_0, 1)$, we get

$$x = x_0 e^{\lambda_2 t}; \qquad y = y_0 e^{\lambda_3 t}; \qquad z = e^{\lambda_1 t}.$$

The solution of the linear system starting at points in Σ pass close the saddle point at the origin and they follow one of the two branches of the unstable 1-dimensional linear manifold. Those points with $x_0 > 0$ (resp. $x_0 < 0$), after the passage close to the origin, leave following the right (resp. the left) branch of $W^u(0, 0, 0)$. The singularity at zero is responsible for an infinite "flight" time near the saddle (points with $x_0 = 0$ are in the 2-dimensional $W^s(0, 0, 0)$). If we look for points in Σ that leave the following the right (or the left) branch of $W^u(0, 0, 0)$, they form a triangle when crossing $x = 1$ (resp. $x = -1$). Let $x_0 > 0$ and consider the right "triangle" of T taken in the $x = 1$ plane. So the first time that the orbit intersects that plane we get the point:

$$x = 1, \qquad y = y_0 x_0^{-\lambda_3/\lambda_2}, \qquad z = x_0^{-\lambda_1/\lambda_2}.$$

Now we will discuss on the global map that describes how the flux maps this "triangle" into a subset of the top square Σ of T. In this way, we define a Poincaré map $F : \Sigma \longrightarrow \Sigma$. Following [6] we put some assumptions on this map. Concretely, we assume that F is defined as $F(x, y) = (f(x), H(x, y))$ where

$$\begin{cases} H(x, y) > 1/4 & x > 0 \\ H(x, y) < -1/4 & x < 0 \end{cases}$$

and where $f : I \longrightarrow I$, $I = [-1/2, 1/2]$, satisfies

1. $f(0^+) = -1/2$
2. $f(0^-) = 1/2$
3. $f'(x) > \sqrt{2}$ for $-1/2 \leq x \leq 1/2$
4. $-1/2 < f(x) < 1/2$ for $-1/2 \leq x \leq 1/2$.

Note that $f'(x) > \sqrt{2}$ implies that f is locally eventually onto. See [6].

Definition 3.1. The map $f : I \longrightarrow I$ is **locally eventually onto** if for any open set $J \subset I$ there exists $k \geq 0$ such that $f^k(I)$ contains $(0, 1)$.

This means that if $J \subset [-1/2, 1/2]$ is any subinterval, then there is an $k > 0$ such that $f^k(J) = [-1/2, 1/2]$. Hence we have chosen $-1/2 \leq x_0, y_0 \leq 1/2$ to simplify our differential equations.

3.2 One-dimensional analysis

In [16], the Lorenz attractor is described as the inverse limit of a semiflow on a two-dimensional smooth branched manifold. Note that this could not be equivalent to the Lorenz attractor obtained in Lorenz equations. To differentiate them we refer as "geometrical Lorenz attractor" the attractor of the Guckenheimer-Williams model. The return map of this semiflow is a discontinuous function $f : I \longrightarrow I$ which satisfies the following properties:

1. f is locally eventually onto.
2. f has a single discontinuity c and is strictly increasing on $[0, c)$ and $(c, 1]$.
3. $f(c^-) = 1$, $f(c^+) = 0$ for $f(0) < c < f(1)$.
4. $f'(x) \longrightarrow \infty$ as $x \longrightarrow c$.

The required properties are inspired in what one observe by numerical computations of the Poincaré map. We saw the numerical results un Fig. 3.2. We have chosen points in $\Sigma \cap \{x = y\}$ between the two fixed points $C_{1,2}$, and we have computed the first return to Σ. Then, we display the x coordinate of the image point versus the x coordinate of the initial point. In plot we display different values of ρ, before and after the creation of the Lorenz attractor. The central plot corresponds to $\rho \approx \rho'$, for which one has a homoclinic orbit. At the exact value ρ' one should have that the two pieces of the image attach to the origin.

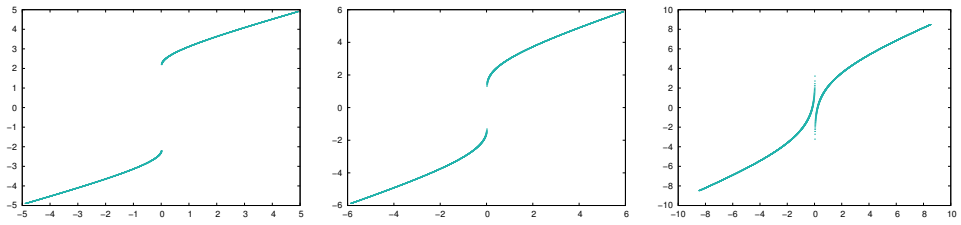

Figure 3.2: Numerical approximation of the Lorenz return map, for $\rho = 10, 13.926$ and 28, from left to right.

To study the dynamics of f, we will use the Kneading invariant of f which, in particular, gives some information about periodic points.

Define a map $K : I \longrightarrow \mathbb{Z}[t]$ given by $K(x) = \sum_{i=0}^{\infty} K_i(x)t^i$ where $K_i(x) = K_0(f^i(x))$ and

$$K_0(x) = \begin{cases} 1 & \text{if } x > c \\ 0 & \text{if } x = c \\ -1 & \text{if } x < c \end{cases}$$

Given a point $x \in I$, $K(x)$ is called the Kneading sequence of x and describes the behaviour of an orbit near the attractor.

We shall compute a truncation of the Kneading sequence from a numerical integration of the Lorenz equations in Chapter 5. Here we use this object to describe the dynamics of the geometric Lorenz attractor of Guckenheimer-Williams model.

With a metric in $\mathbb{Z}[t]$, for example, with the metric induced by the distance

$$d\left(\sum_{i=0}^{\infty} \theta_i t^i, \sum_{i=0}^{\infty} \theta_i' t^i\right) = \sum_{i=0}^{\infty} |\theta_i - \theta_i'| 2^{-i},$$

there exist $\lim_{y \longrightarrow x^+} K(y) = K(x^+)$ and $\lim_{y \longrightarrow x^-} K(y) = K(x^-)$, and we call $(K_+, K_-) = (K(c^+), K(c^-))$ the Kneading invariant of f.

D. Rand in [12] proves that there is a one-to-one map between a point $x \in I$ and a formal power series $\theta = \sum_{i=0}^{\infty} \theta_i t^i$ with $\theta_i \in \{-1, 0, 1\}$ if θ is (K_+, K_-)-admissible. We say that θ is (K_+, K_-)-admissible if for all $n \geq 0$ satisfies

1. $K_+ - 1 < \sum_{i=n}^{\infty} \theta_i t^{i-n+1} < K_- + 1$ and,
2. either $\sum_{i=n}^{\infty} \theta_i t^i = 0, K_- > \sum_{i=n}^{\infty} \theta_i t^{i-n}$ or $\sum_{i=n}^{\infty} \theta_i t^{i-n} > K_+$.

As a consequence, a θ periodic (K_+, K_-)-admissible power series corresponds to a periodic point of f with (K_+, K_-) kneading invariant of f. In particular, since the Lorenz system has a symmetry, one has that $K_+ = -K_-$.

Then, if θ is a formal power series which satisfies

$$\left|\sum_{i=n}^{\infty} \theta_i t^{i-n}\right| > K_+ \text{ or } \sum_{i=n}^{\infty} \theta_i t^i = 0, \tag{3.1}$$

also satisfies conditions 1. and 2. and hence θ is (K_+, K_-)-admissible.

Summarizing, the map $x \longmapsto K(x)$ induces a one-to-one map between the periodic points of f and a periodic $\theta = \sum_{i=0}^{\infty} \theta_i t^i$ with $\theta_i \in \{-1, 0, 1\}$ which satisfy 3.1 for all $n \geq 0$.

One can also prove using Kneading invariant that for $\frac{\partial f}{\partial x} > \sqrt{2}$, the periodic points of f are dense in I, and that periodic points determine K_+ and K_-, see [12].

One of the properties of a one-dimensional chaos is that the set of periodic orbits is dense, [4]. In particular, we will see that for the tent map in section 4.5, that will allow us to deduce that the strange attractor is chaotic for classical parameters $\sigma = 10, \beta = 8/3$ and $\rho = 28$.

3.3 Recovering the Geometric Lorenz attractor

We have seen how to pass from a 3-dimensional flow defined by the Lorenz equations to a 2-dimensional Poincaré map $P : \Sigma \longrightarrow \Sigma$, and then to a 1-dimensional map $f : I \longrightarrow I$. This process is reversible, so we will study now how to recover the geometric Lorenz attractor from the attractor of the Poincaré map. In the next chapter we shall discuss how to recover the Lorenz attractor in Lorenz equations from the Guckenheimer-Williams model.

We will make some assumptions about the flow. The first of these assumptions is that the eigenvalues of the origin satisfy $0 < -\lambda_1 < \lambda_2 < -\lambda_3$, that is, that the linear dynamics around the saddle is like the one that we have in Lorenz equations. The second assumption is that there exist a family $\mathcal{F}$ of leaves in Σ such that $\mathcal{F}$ is invariant under the return map F. In the next chapter we shall discuss details of this foliation (see Definition 4.2 for a definition of foliation and the smoothness required). That is, if $\gamma \in \mathcal{F}$ then F is defined in γ and $F(\gamma) \in \mathcal{F}$. The family $\mathcal{F}$ is part of a strong stable foliation for the flux defined in a neighbourhood of the attractor. Also we assume that all points of $\Sigma \backslash \{x = 0\}$ return to Σ and the return map F is sufficiently expanding in the transverse direction to the leaves of $\mathcal{F}$. Finally, we assume that the flux is symmetric with respect to a rotation around the z-axis.

Note that all of these hypothesis are satisfied by the Lorenz equations for $\sigma = 10, \beta = 8/3$ and $\rho = 28$. The second assumption was proved by W. Tucker in [14] and the first and last assumptions have been already seen in this work.

Analytically, these assumptions can be rewritten using a system of coordinates (x, y) on Σ, such that F has the following properties:

1. The leaves of $\mathcal{F}$ are given by x equals a constant, with $-1/2 \leq x \leq 1/2$.
2. There exist functions f and g such that $F(x, y) = (f(x), g(x, y))$ for $x \neq 0$ and such that $F(-x, -y) = -F(x, y)$.
3. $f'(x) > \sqrt{2}$ for all $x \neq 0$ and $\lim_{x \longrightarrow 0} f'(x) = \infty$.
4. $\frac{\partial g}{\partial y}(x, y) < \delta < 1$ for all $x \neq 0$ and $\lim_{x \longrightarrow 0} \frac{\partial g}{\partial y}(x, y) = 0$ independently of y.

Note that F is not defined for $x = 0$ and as conditions 3. and 4. are satisfied, there exist a hyperbolic structure, defined on the invariant set (the attractor) of the system. Let us recall what is referred as hyperbolic structure, see [2] for further details.

Definition 3.2. Let Λ be an invariant set for the discrete dynamical system defined by $F : \mathbb{R}^n \longrightarrow \mathbb{R}^n$. A **hyperbolic structure** for Λ is a continuous invariant direct sum decomposition $T_\Lambda \mathbb{R}^n = E^u_\Lambda \oplus E^s_\Lambda$, with the property that there are constants $C > 0$, $0 < \lambda < 1$, and $k > 0$ such that:

- if $v \in E^u_x$, then $|DF^{-k}(x)v| \leq C\lambda^k |v|$;
- if $v \in E^s_x$, then $|DF^k(x)v| \leq C\lambda^k |v|$.

Moreover, only a countable union of vertical leaves in Σ have trajectories that ends on $x = 0$, while all the other trajectories remain inside Σ. Therefore, any invariant set of F will have a suitable defined hyperbolic structure and be attracting.

Let $r^\pm$ and $t^\pm$ such that $\lim_{x \longrightarrow 0^-} F(x,y) = (r^+, t^+)$ and $\lim_{x \longrightarrow 0^+} F(x,y) = (r^-, t^-)$. Due to the assumption 4. on the behaviour of the derivatives of $g(x,y)$ the limits exist. As the condition 4. is satisfied, the set $V = \{(x,y) : r^- \leq x \leq r^+\} \backslash \{x = 0\}$ is mapped into itself. In this way, with the exception of points in a zero measure set, all points of Σ have orbits that eventually enter in V and then remain there when F is iterated. So V is a positive invariant set for F.

Let $A = \bigcap_{n \geq 0} F^n(V)$. As said, all points of V tend to A or have orbits that end on $\{x = 0\}$. If we provide that the images of U are dense in A, we can assert that A is an attractor for the map F since then A will contain a transitive orbit. This will guarantee the indecomposable property required in the definition of attractor, see Definition 1.7.

Proposition 3.3. *Let $x \in A$ and consider a neighbourhood $U \subset A$ of x. Then the $\{F^k(U), k \geq 0\} \subset A$ is a dense set.*

Proof. We show that exists an integer n with $f^n(J) = (r^-, r^+)$ for any interval $J \subset (r^-, r^+)$ and $0 \notin J$. Then we choose any points $x \in A$ and we shall locate a point of $U \subset A$ whose orbit passes within distance $\varepsilon > 0$ of x, for a given ε. This proves that the image of U are dense in A.

Since $0 \notin T$, $f(J)$ is connected. If $0 \notin f(J)$, we replace J by $f(J)$ which satisfies $\frac{l(f(J))}{l(J)} > \sqrt{2}$, ($l(J)$ is the length of the interval J) from property 3. and consider $f^2(J)$.

If $0 \in f(J)$ then $f^2(J)$ has two components and one of these components must be longer that J because $(f^2)' > 2$ from property 3. and the chain rule. Then we replace I by the longer component of $f^2(J)$ and continue the argument.

Since J has a finite length, there exists an integer n with $f^n(J) = (r^-, r^+)$. Then we choose any points $x \in A$.

For (x', y_1) and $(x', y_2) \in \Sigma$ we obtain $d(F^n(x', y_1), F^n(x', y_2)) < \delta^n |y_1 - y_2|$ as a result of apply properties 2. and 4.. And consequently, given any $\varepsilon > 0$ we can find m such that

$d(F^m(x', y_1), F^m(x', y_2)) < \varepsilon$. Since $x \in A$ there is a point $(u, v) \in \Sigma$ such that $F^m(u, v) = x$.

Given n, w then there is a point $(x', y') \in U$ such that $F^n(x', y') = (u, w)$ and then $d(F^m(u, w), F^m(u, v)) = d(F^{m+n}(x', y'), x) < \varepsilon$.

□

To describe the topology of A we will consider now the orbits that tends to $\{x = 0\}$ by defining a new map $G : V \backslash \{x = 0\} \longrightarrow V$, such that $G(x, y) = (f(x), h_x(y))$, where $h_x(y) = \alpha y - \text{sign}(x)\beta$, $0 < \alpha < 1/2$ and β is chosen such that G is a one-to-one map. Using the properties of f described above, we deduce that $G^n(V)$ consists of a certain number or rectangles. Moreover, $\Gamma = \bigcap_{n \geq 0} G^n(V)$ will be an attractor of the points of V.

Topologically, A can be obtained from Γ, by pinching together vertically all the points which lie in the image of a vertical segment $\{G^n(u, v) : u = r^{\pm}\}$.

Note that since the preimages $f^{-n}(0)$ are dense in (r^-, r^+), by arbitrarily small adjustments in the mapping f, we can arrange that the f orbits of the points $r^{\pm}$ ends at 0. Those are the homoclinic orbits inside the attractor.

Finally, the geometric Lorenz attractor can be obtained from A. This construction is quite involved and used the existence of the strong foliation of the geometrical model. We do not provide further details here, but these can be found in the work of Gukenheimer and Williams [6], [16] and [5].

Chapter 4

Strange attractor

Many authors have performed numerical simulations of the Lorenz equations, and provide evidence that the Lorenz system contains an attractor for ρ between 13.926 and 31.01. On the other hand, to prove the existence of Lorenz attractor requires to prove that the system admits a strong stable foliation transversal to the restriction of the vector field at the points (in a neighbourhood) of the attractor.

In this chapter we start by considering a hyperbolic attractor. In this case, we will see that there exists a transversal strong stable foliation. But the Lorenz attractor is not hyperbolic, since it contains a singular point, so we will discuss the existence of such a foliation for the Lorenz system.

In particular, for the classical parameters of Lorenz, $\sigma = 10, \beta = 8/3$ and $\rho = 28$, W. Tucker [14], proved the existence of the strong stable foliation and, in turn, that the strange attractor of Lorenz system is equivalent to a geometrical Lorenz attractor. That is, it is equivalent to the attractor obtained in a geometrical model as considered in the previous chapter.

Moreover, it will be shown that the Lorenz attractor is robust since, for small perturbations, hyperbolicity guarantees the persistence of transversal strong stable foliation .

4.1 Hyperbolic attractors

Definition 4.1. An attractor $A \in M$ of a dynamical system, defined by a smooth vector field F with evolution operator ϕ, is called **hyperbolic** if for each $p \in A$ there exists a splitting of the tangent space $T_p(M) = E^u(p) \oplus E^c(p) \oplus E^s(p)$ with the following properties:

1. The linear subsets $E^u(p), E^c(p)$, and $E^s(p)$ depend continuously on p whereas their dimensions are independent of p.

2. For any $p \in A$, the linear subspace $E^c(p)$ is 1-dimensional and generated by $F(p)$.

3. The splitting is invariant under the derivative $d\phi_t$ in the sense that for each $p \in A$ and $t \in \mathbb{R}$:

$$d\phi_t(E^u(p)) = E^u(\phi_t(p)), \qquad d\phi_t(E^c(p)) = E^c(\phi_t(p)), \qquad d\phi_t(E^s(p)) = E^s(\phi_t(p)).$$

4. The vectors $v \in E^u(p)$ (respectively $E^s(p)$), increase (respectively, decrease) exponentially under application of $d\phi_t$ as a function of t, in the following sense. Constants $C \geq 1$ and $\lambda > 1$ exist, such that for all $0 < t \in \mathbb{R}$, $p \in A$, $v \in E^u(p)$, and $w \in E^s(p)$, we have:
$$|d\phi_t(v)| \geq C^{-1}\lambda^t|v| \qquad \text{and} \qquad |d\phi_t(w)| \geq C\lambda^{-t}|w|$$
where $|\cdot|$ is the norm of tangent vectors.

One of the tools used to provide persistence of hyperbolic attractors is the existence of a stable foliation. We will see first a general definition, based on [2], of a foliation of a manifold V, which is a decomposition of V in lower-dimensional manifolds, called the leaves of the foliation.

Definition 4.2. Let V be a m-dimensional $\mathcal{C}^\infty$-manifold. A C^l-**foliation** of V by C^k h-dimensional leaves is a map
$$\mathcal{F} : v \in V \longmapsto F_v,$$
where F_v is an injectively immersed submanifold of V containing v, in such a way that for certain integers k, l, and h ($h \leq m$) one has

1. If $w \in F_v$, then $F_v = F_w$.
2. For each $v \in V$ the manifold F_v is of class $\mathcal{C}^k$.
3. For any $v \in V$ there exist $\mathcal{C}^l$-coordinates $x = (x_1, \cdots, x_m)$, defined on a neighbourhood $V_v \in V$ of v, such that for any $w \in V_v$, the connected component of $F_w \bigcap V_v$, has the form
$$\{x_{h+1} = x_{h+1}(w), \cdots, x_m = x_m(w)\}.$$

In the case of Lorenz equations, the existence of such a foliation will be done over V, where V is the Poincaré section $\Sigma = \{z = \rho - 1\}$ introduced in Section 3.1. One can define a hyperbolic attractor for discrete dynamical systems. The formal definition is similar to the Definition 1.2 above, but in this case the evolution operator is defined in terms of the iterates of the map, and the splitting of the tangent space is of the form $E^u(p) \oplus E^s(p)$ (there is no central direction). The Lorenz attractor turns out to be hyperbolic for the Poincaré map.

The hyperbolicity of the Lorenz attractor is a consequence of the existence of a strong stable foliation. Here we introduce what we understand by foliation. We say that two points $v, w \in U$ belong to the same stable equivalence if

$$\lim_{t \longrightarrow \infty} \rho(\Phi_t(v), \Phi_t(w)) = 0.$$

where ρ is a distance function on M, and Φ_t is an evolution operator as in def. 1.2. For a hyperbolic attractor A, it can be shown that the connected components of the equivalence

classes of the stable equivalences are leaves of a foliation in a neighbourhood $U \supset A$, such that $\Phi_t(U) \subset U$ for $0 < t \in T$ and $\bigcap_{0<t\in T} \Phi_t(U) = A$. This is called the **stable foliation**, denoted by $\mathcal{F}^s$. Some properties of the stable foliation are described in the following theorem, which can be found in [2].

Theorem 4.3. *For a hyperbolic attractor A of a dynamical system with time maps ϕ_t and a neighbourhood $U \supset A$, such that $\phi_t(U) \subset U$ for $0 < t \in T$ and $\bigcap_{0<t\in T} \phi_t(U) = A$. Then for the stable foliation $\mathcal{F}^s$ one has*

1. *The leaves of $\mathcal{F}^s$ are manifolds of dimension equal to $dim E^s(p)$, $p \in A$, and of differentiability equal to that of ϕ_t.*
2. *At each point $p \in A$ one has that $T_p\mathcal{F}^s(p) = E^s(p)$.*
3. *$\mathcal{F}^s$ is of class $\mathcal{C}^0$.*
4. *For any $p \in U$ and $0 < t \in T$ one has that $\phi_t(\mathcal{F}^s(p)) \subset \mathcal{F}^s(\phi_t(p))$ that is, the foliation is invariant under the forward dynamics.*

For Lorenz equation, the leaves of this foliation are 1-dimensional, and consequently $\mathcal{F}^s$ is $\mathcal{C}^1$.

Since the Lorenz equations has a singular point at $(0, 0, 0)$, the Lorenz attractor is no hyperbolic but it is a partially hyperbolic set for ODE's system. More concretely, it is a singularly hyperbolic attractor (it contains singularities which are hyperbolic points).

Definition 4.4. A compact invariant set Λ of X is **partially hyperbolic** if there exists a continuous dominated splitting $T_\Lambda M = E^s \oplus E^u$ such that E^u contains the direction of the flow and E^s is one-dimensional and contracting. That is, they are constants $0 < \lambda < 1$, $c > 0$ and $T > 0$ such that

$$||dX_t/E^s|| \cdot ||dX_{-t}/E^u|| < c\lambda^T, \qquad ||dX_t/E^s|| \leq c\lambda^T.$$

So in this case, we cannot claim that the stable foliation exists for the Lorenz attractor. But for classical values of the parameters, it has been proved the existence of a strong stable foliation [14], and therefore, that the Lorenz system contains a strange attractor.

Remark 4.5. In the literature one can find other types of strange attractors. There are examples of uniformly hyperbolic attractors (e.g. the so-called Plykin attractor). Also there are examples of non-hyperbolic (e.g. the Hénon attractor). In particular, these last type of attractors are no robust with respect to changes in the parameters and/or perturbations.

4.2 Computer assisted proof

W. Tucker combines rigorous proofs with the construction of a numerical method to proof the existence of a strong stable foliation in the Lorenz system. Using interval arithmetic with directed rounding eliminates the problem of control rounding errors.

He uses the classical Euler method applied to the Lorenz equations, so that he obtain an interval solution that contains the right solution. The numerical method implemented proves the following statements:

1. The return map $F : \Sigma \longrightarrow \Sigma$, $\Sigma := \{z = \rho - 1\}$, is well defined for the geometric model. F is not defined on the line $\Gamma = \Sigma \cap W^s(0)$.

2. There exists a compact subset $S \subset \Sigma$ such that $S \backslash \Gamma$ is forward invariant under F. That is $F(S \backslash \Gamma) \subset S$.
   S is a trapping region, see Section 1.2. This ensures that the flow has an attracting set $\mathcal{A}$ with a large basin of attraction. In particular

   $$\Lambda = \mathcal{A} \bigcap \Sigma = \bigcap_{n=0}^{\infty} F^n(S)$$

   is an attracting set for F.

3. On S, there exists a cone field $\mathfrak{C}$ which is mapped strictly into itself by DF. A cone field is a smooth map that associate a cone $\mathfrak{C}_x$ to a given point $x \in S$. That means $DF(x)\mathfrak{C}_x \subset \mathfrak{C}_{F(x)}$, for all $x \in S$. The computation of $DF(x)$ requires the integration of the variational equations.

4. The tangent vectors in $\mathfrak{C}$ are eventually expanded under the action of DF: there exists $C > 0$ and $\lambda > 1$ such that for all $v \in \mathfrak{C}_x$, $x \in S$, we have

   $$|DF^n(x)v| \geq C\lambda^n |v|, \qquad n \geq 0.$$

These conditions imply the existence of a dense orbit in Λ, hence Λ is an attractor, see definition 1.7. As a consequence of 3. and 4., we have that the return map F has an invariant stable foliation. We refer to [10] for related comments.

W. Tucker constructs the set S by the finite union of rectangles S_i, all included in the plane Σ. He consider the Lorenz equations with the classical parameters $\sigma = 10$, $\beta = \frac{8}{3}$ and $\rho = 28$.

Due to the symmetry of the Lorenz equations, it is only needed to compute one of the branches $x > 0$ or $x < 0$, to reduce the running time. Each rectangle S_i is associated with a constant cone, identified for two vectors and such that contains the tangent vectors of the flow for all points in S_i.

Initially the algorithm starts from the rectangles S_i in the chosen branch and from the associated cones located in the return plane $\Sigma = \{z = \rho - 1 = 27\}$.

To compute one iterate of the Poincare map a sequence of local Poincaré map $\Pi_k : \Sigma^{(k)} \longrightarrow \Sigma^{(k+1)}$ is computed (parallel shooting), where $\Sigma^{(0)} = \Sigma$ and the last one returns to Σ. The plane $\Sigma^{(k+1)}$ is defined such that it contains the vector e_j, $j = 1, 2, 3$, associated to the direction of the component of maximum modulus of the vector field. In this way a pseudo-

path between return planes $\Sigma^{(k)}$, which are either (x, y)-plane, (y, z)-plane or (x, z)-plane, is constructed. Using the pseudo-path as an initial guess, one can prove the existence of a true solution of the system.

The main idea is the following. While applying Π_1 to an initial rectangle S_i, here denoted as $R^{(0)}$, we get a rectangle $R^{(1)}$ in the plane $\Sigma^{(1)}$. If Π_1 is computed using interval arithmetic one gets the rectangular hull of the largest image of S_i. $R^{(1)}$ is then flowed to $\Sigma^{(2)}$ and we obtain the rectangle $R^{(2)}$ in the plane $\Sigma^{(2)}$ and so on. Generally,

$$\Pi_k(R^{(k)}) \subseteq R^{(k+1)}.$$

If the rectangles obtained grow too much, then they are divided in smaller rectangles and, for each rectangle, the local Poincaré map is applied. When computing the complete return map F, the initial rectangle S_i is contained in the union of overlapping rectangles.

This algorithm is not applied near to the origin. In particular, it is applied outside of a small cube centered at the origin. Inside this cube, Tucker uses a local map similar to the on shown in Section 3, Fig. 3.1. However, instead of using a local map, a change of variables is applied to the Lorenz equations to get a normal form, to avoid difficulties on the computation near to the origin. When an orbit arrives to the cube, the program computes the image of the orbit when it comes out of the cube, and it continues with the algorithm.

This procedure ends after n_0 steps such that $R^{(n_0)}$ is contained in Σ. The result obtained is a finite set of overlapping rectangles that contains S_i. Therefore, we can rigorously check that S verify $F(S\backslash\Gamma) \subset S$. In this way, 1. and 2. were proved.

For quantifying the hyperbolic properties of the return map, each initial rectangle S_i comes with a cone $\mathfrak{C}_{[\alpha_i]}$, where $[\alpha_i] = [\alpha_i^-, \alpha_i^+]$, α_i^- is the angle between the vector u_i and the x-axis and α_i^+ is the angle between the vector v_i and the x-axis. Both u_i and v_i are the tangent vectors. Hence we want to compute the evolution of the tangent vectors associated to each rectangle. In each step k, the two vectors located in $\Sigma^{(k)}$ are translated to $\Sigma^{(k+1)}$. An enclosure cone $\mathfrak{C}^{(k+1)}$ of the image of $\mathfrak{C}^{(k)}$ over $D\Pi_k$, is evaluated. It is also computed using interval arithmetic with directed rounding.

If the enclosure of the cone $\mathfrak{C}^{(k+1)}$ gives new cones, associated to rectangles S_k, that are not contained in S, then one verify if these cones are included in $\mathfrak{C}^{(k)}$. If not, we wide the associated cone with S_k and recompute the information of S_k with the new cone. Therefore, when the process ends, for all S_i of S,

$$F(S_i) \cap S_k \neq 0 \implies DF(S_i)\mathfrak{C}_{[\alpha_i]} \subset \mathfrak{C}_{[\alpha_i]}.$$

That gives the proof of the existence of a forward invariant cone field, and therefore 3. is proved.

Respect to the range of expansion of the cone field $\mathfrak{C}$, W. Tucker take the following con-

siderations respect to the cones in each step:

(a) The vectors $u^{(k+1)}$ and $v^{(k+1)}$ have the maximum angle, which guarantee that the resultant cone $\mathfrak{C}^{(k+1)}$ contains the images of the tangent vectors of the initial cone.

(b) For each step and each cone associated to a rectangle, the algorithm estimates the expansion of the angle of the cone. When the algorithm ends and arrives again to Σ, the estimate of the expansion of a cone associated to a rectangle is the product of the estimations done in each step.

(c) And finally, an estimation $\mathcal{E}_i^{(k)} \geq 1$ of the expansion of the cones is the minimum of the estimations computed for all the vectors of the cone associated to S_i.

Therefore, any tangent vector $v \in \mathfrak{C}_{[x_i]}$ following the orbit of an initial point $x_0 \in S_i$ will satisfy

$$|DF^n(x_0)v| \geq |v| \prod_{k=0}^{n-1} \mathcal{E}_i^{(k)}.$$

W. Tucker proves that the expansion along orbits in S grows exponentially with the number of iterates and as consequence, 4. is verified.

To sum up, the flow of the Lorenz equations is uniformly volume-contracting and transverse to S. An iterate of the return map F contracts area on S. This property together with the existence of the forward invariant unstable cone field implies that F admits an invariant stable foliation with $\mathcal{C}^1$ leaves, see definition 4.2.

4.3 Robustness

The existence of the stable foliation establishes the robustness of the Lorenz attractor in the sense that it is stable for small perturbations. Concretely, the following theorem is stated in [2].

Theorem 4.6. *(Persistence of hyperbolic attractor)*
Let (T, M, ϕ_t) a dynamical system with time-t maps ϕ_t, and let A be a hyperbolic attractor of this system. Then there exists a neighbourhood $\mathcal{U}$ of the evolutionary process ϕ (in the $\mathcal{C}^1$-topology), and a neighbourhood $V \subset M$ of A, such that $\phi_t(V) \subset V$ for all $0 < t \in T$ and $A = \bigcap_{0<t\in T} \phi_t(V)$, and such that for all evolutionary process $\widetilde{\phi} \in \mathcal{U}$:

1. *$\widetilde{A} = \bigcap_{0<t\in T} \widetilde{\phi}_t(V)$ is a hyperbolic attractor of $\widetilde{\phi}$.*
2. *There exists a homeomorphism $h : A \longrightarrow \widetilde{A}$, that conjugates $\phi|_A$ and $\widetilde{\phi}|_{\widetilde{A}}$.*

In general, for parameters that are not in the neighbourhood $\mathcal{U}$, we cannot claim that there exists a stable foliation. For the Lorenz system the previous theorem guarantees the existence of an hyperbolic attractor for parameter values closed to the classical ones. Since the

foliation is needed to be transverse to the attractor, some works have been recently done, studying the values of ρ such that this transverse condition is lost. The most accurate value is given by [3], which claim that for $\rho > 31.01$ the foliation is non-transverse to the attractor.

4.4 Dynamics of Lorenz attractor

Once we have seen the existence of a strong stable foliation, in this section it will be discussed how this foliation let us analyse the dynamics of the Lorenz system using a one-dimensional function.

Suppose there exists $\mathcal{F}$ the $\mathcal{C}^1$ strong stable foliation of the Lorenz attractor with γ_x leaves tangent to the directions of strongest conditions. This leaves satisfies the equivalence relation $x \sim y$ if and only if $\gamma_x = \gamma_y$.

Then, given $x \in \mathbb{R}^3$, there exists a unique $\gamma_x \in \mathcal{F}$ such that $x \in \gamma_x$. Let Σ be the Poincaré hyperplane. Consider $\mathcal{F}|_\Sigma = \bigcup_{x\in\Sigma} \gamma_x$ the restriction to Σ of the foliation. Then we can define

$$\begin{aligned} \widetilde{f} : \mathcal{F}|_\Sigma &\longrightarrow \mathcal{F}|_\Sigma \\ \gamma &\longmapsto \widetilde{f}(\gamma) = \{\gamma_{P(x)}, x \in \gamma\} \end{aligned}$$

where $P(x)$ is the image of x by the Poincaré map.

As $\mathcal{F}|_\Sigma$ is transversal to $I = \{y = z = 0, x \in [-r, r]\}$ ($r > \sqrt{\beta(\rho-1)}$), we can define $f : I \longrightarrow I$, where $f(x) \in \Sigma$ is the unique point such that $\gamma_{f(x)} = \widetilde{f}(\gamma_x)$.

Then, if this strong stable foliation exists, is transversal and contractile, the one dimensional dynamics of f is equivalent to the dynamics of the Lorenz attractor.

All this arguments justify that the one dimensional dynamics of f is equivalent to the dynamics of the Lorenz attractor if the strong stable foliations exists and is transversal and contractile. We have seen in section 4.2 that this stable foliation exists for the classic parameters of σ, β and ρ and for $\Sigma = \rho - 1$.

Since the Lorenz attractor is hyperbolic for the flow in $\mathbb{R}^3 \backslash \{(0,0,0)\}$, every Poincaré hyperplane Σ, that does not contain the singular point, has the same behaviour. Therefore we study in the following section another relevant Poincaré map.

4.5 Tent map

To study the Lorenz system, E. Lorenz in [9] defined z_n to be the nth local maximum of $z(t)$, and plotted z_{n+1} versus z_n. This map corresponds to a Poincaré section $\Sigma := \{(x, y, z) \in \mathbb{R}^3 : \dot{z} = 0, \ddot{z} < 0\}$. We plot in Figure 4.1 a Poincaré map $P : \Sigma \longrightarrow \Sigma$.

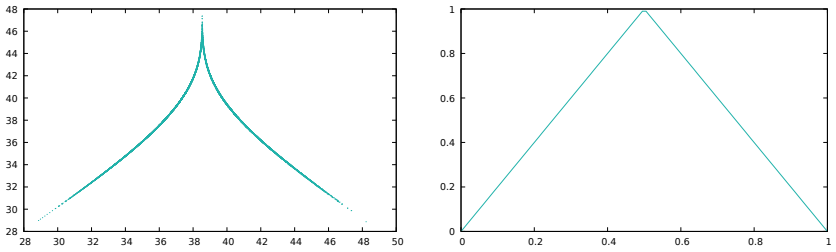

Figure 4.1: Left, we the plot z_{n+1} versus z_n. Right, we plot the Tent map

Based on these numerical studies, E. Lorenz observed that this map is similar to the so-called tent map. Actually the Poincaré map is topologically equivalent to the tent map, therefore some properties of the Lorenz system can be related to the properties of the tent map, which are studied in this section.

The tent map $T_2 : I \longrightarrow I$ is an application in $I = [0, 1]$ defined as

$$T_2(x) = 1 - |1 - 2x|$$

Note that T_2 is $C^1(I \backslash \{1/2\})$.

The Lyapunov exponent gives the rate of exponential divergence from two close initial conditions. Let us recall what is referred as Lyapunov exponent.

Definition 4.7. Let $f : I \longrightarrow I$ be a C^1 function and x_0 some initial condition, the **Lyapunov exponent** is defined as

$$\lambda(x_0) = \log \lim_{n \longrightarrow \infty} \sum_{i=0}^{n-1} \log \left| f'(x_i) \right|,$$

where $x_i = f^{(i)}(x_0)$ are the points of orbit of x_0.

Let x_0 be some initial condition and consider the orbit of a nearby point $x_0 + \delta_0$ where δ_0 is very small. Let δ_n be the separation in the two orbits after n iterates. If $|\lambda_n| \approx |\delta_0| e^{n\lambda}$, then λ is the Lyapunov exponent. A positive Lyapunov exponent means that orbits separate exponentially fast, which is sufficient to show that the system displays sensitive dependence on initial conditions. The Lyapunov exponent of the tent map for all x_0 such that its orbit $O(x_0)$ is not eventually periodic can be easily computed. Observe that $x_0 = 0$ is a stationary point, and $x_0 = 1$ or $x_0 = \frac{1}{2}$ are eventually stationary points. We consider $x_0 \neq \frac{1}{2}$, therefore $|T_2'(x_0)| = 2$. Thus

$$\lambda(x_0) = \log 2.$$

As the Lyapunov exponent of the tent map is always positive, the tent map contains chaotic orbits.

Moreover, the tent map has periodic orbits of all periods. The plots on Fig. 4.2 shows that T_2 has exactly 2^n periodic points of period n. Then the number of stationary points $\mathrm{Fix}(T_2^n)$ in T_2^n is 2^n. Particularly, the union of $k-1$ stationary points $\mathrm{Fix}(T_2^n)$ is $\sum_{n=1}^{k-1} 2^n = 2^k - 2$. Therefore there exist a periodic orbit of minimal period k, for all $k \geq 0$.

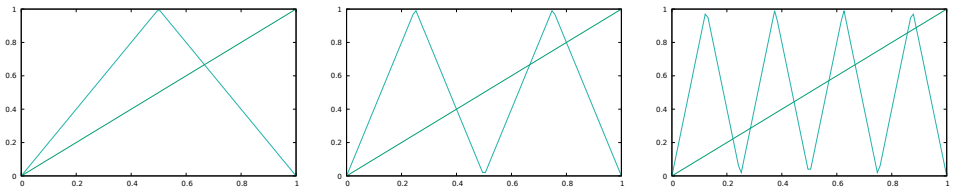

Figure 4.2: Representation of the 2^n periodic points of T_2^n, for $n = 1, 2$ and 3.

Since the one dimensional dynamics of f, defined in Section 4.4, is equivalent to the dynamics of the Lorenz attractor, we can conclude that the properties we have studied for the tent map can be applied to the Lorenz system.
Indeed, the Lorenz system has a positive Lyapunov exponent, which means that the system displays sensitive dependence on initial conditions. The maximal Lyapunov exponent for the Lorenz system is known to be about 0.9056, see [15].

Chapter 5

Kneading theory

In this chapter we will study the topologically classification of the orbits in the Lorenz equations using symbolic dynamics.

C. Sparrow introduced this concept in [13], but we will base this study in [1], where from an approximation of the Kneading invariant value it can be shown which Lorenz attractors are topologically conjugated.

5.1 Kneading invariant

The Lorenz attractor undergoes a homoclinic bifurcation (See section 2.3) when the separatrices of the origin change the behaviour from the spirals around $C1$ and C_2 to cross over to the other stationary point.

The symmetry of the Lorenz equations, $(x, y, z) \longrightarrow (-x, -y, z)$ define two sides of a separatix. The flux has an alternative sign in the x-axis that suggest the introduction of a symbolic dynamic, $\{\pm 1\}$-based alphabet to be employed for the symbolic description of the separatrix.

The symbolic dynamics defined before has a feature that on one side, the orbit spirals around the point C_1 and on the other side, the orbit spirals around the point C_2. We assign the value $+1$ around C_1, and -1 around C_2 and then we can talk about the right separatrix and left separatrix respectively.

Due to the symmetry of the Lorenz mapping $x_{n+1} = T(x_n) = T^n(x_0)$ from the Lorenz map $T(x) = \text{sign}(x) \cdot (-1 + \beta|x|^\alpha)$, forward iterates of the right separatrix O^+, of the discontinuity point are detected to generate a kneading sequence $\{k_n(O^+)\}$ defined by the following rule:

$$k_n(O^+) = \begin{cases} +1, \text{ if } T^n(O^+) > 0, \\ -1, \text{ if } T^n(O^+) < 0, \\ 0, \text{ if } T^n(O^+) = 0, \end{cases} \tag{5.1}$$

here $T^n(O^+)$ is the n-th iterate of the right separatrix O^+ of the origin. The condition $T^n(O^+) = 0$ is interpreted as the homoclinic orbit.

A kneading invariant is a value that is intended to uniquely describe the complex dynamics of the system that admits a symbolic description using two symbols $\{\pm 1\}$. In a symmetric system with the Lorenz attractor, the kneading invariant is assigned to quantify the symbolic description of either separatrix. Thus, it reflects quantitatively a qualitative change in the separatrix behaviour, such as flip-flopping patterns, as the parameter of the system is changed.
The kneading invariant for the separatrix is defined in the form as a power series:

$$P(q) = \sum_{n=0}^{\infty} k_n q^n.$$

Setting $q \in (0, 1)$ make the above series convergent.
The kneading invariant depends on parameters of Lorenz equations, hence two systems of Lorenz equations can be compared and classifies as its value of kneading invariant.
Two systems with the Lorenz attractors are topologically conjugate when they have the same kneading invariant.

5.2 Topologically equivalent systems

In this section we will see the Kneading invariant over to numerical studies in the Lorenz equations, reproducing the work of R. Barrio in [1].
Up to here we have study the Lorenz system while the parameter ρ changes. Now, we will vary ρ and σ to get the Kneading invariants.

In this computational study we will take the Lorenz equations with a fixed initial condition, and as the parameters ρ and σ are changed, its Kneading sequence and Kneading invariant will be approximated.
We start by taking a specific range in the (ρ, σ)-space, for example $[10, 150]$ for ρ and $[1, 80]$ for sigma, and we scan a grid of 1000×1000 points uniformly distributed over these ranges. For each pair (ρ, σ), integrate the Lorenz equations, using a Taylor series method, with initial conditions (x_0, y_0, z_0) in the unstable manifold of the origin as in section 2.2. During the integration, we identify and record the first 50 values of the Kneading sequence $\{k_n\}_{50}$, and compute the partial kneading power series $P_{50}(q) = \sum_{n=0}^{50} k_n q^n$, where q is set to be 0.5.

Hence we have defined a bi-parametric mapping $(\sigma, \rho) \longrightarrow P_{50}(q)$. We represent in Fig. 5.1 the Kneading-based color scan of the dynamics of the Lorenz equations mapped onto

the (ρ, σ)-parameter plane. Each value of the Kneading invariant is assigned to a color of a given palette colors. We use an adjusted logarithmic function applied to the Kneading invariant to get a graphic representations as it is shown in Fig. 5.1.

Note that we are just taking in consideration the first 50 values, so we cannot guarantee that two systems are topologically conjugated. We only have a numerical evidence that they could be equivalent.

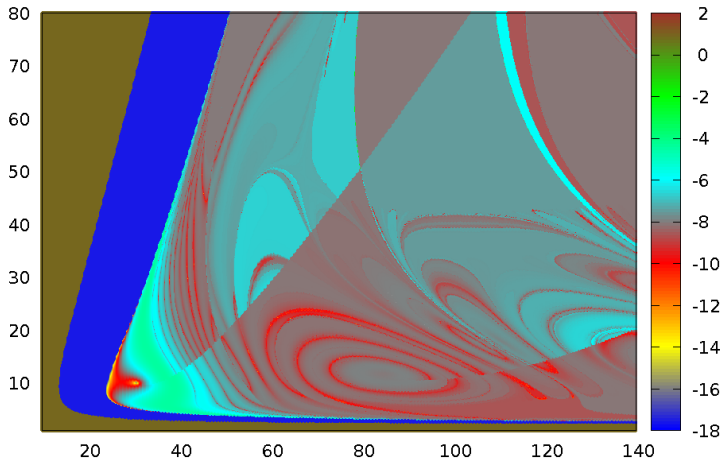

Figure 5.1: Numerical approximation of the Kneading invariant on the (ρ, σ), see text for details

Based on this map, we can study which Lorenz attractors are topologically conjugated since R. F. Williams proved in [16] that the kneading sequences are topological invariants. In the following theorem, $\mathcal{L}$ denotes an open set of vector fields of $\mathbb{R}^3$ which, in particular, contains all the vector fields generated by the Lorenz equations for parameters σ, β and ρ for which there is a Lorenz-like attractor. In particular, for the classical parameters σ and β, this range includes values of ρ between 13.926 and 31.01, which corresponds to the homoclinic orbit and the loss of tangency as we have explained in sections 2.3 and 4.3.

Theorem 5.1. *There is a positive number Δ, such that, if the attractors A_X and A_Y, for $X, Y \in \mathcal{L}$, are homeomorphic via a homeomorphism within Δ of the identity (C^0-sense), the X and Y have the same kneading sequences.*

Δ depends on the parameters σ, β and ρ and delimits the size of the zone, around the stationary point, where the homeomorphism is close to the identity.
Since there exists a homeomorphism between A_X and A_Y, these attractors are said to be topologically conjugated.

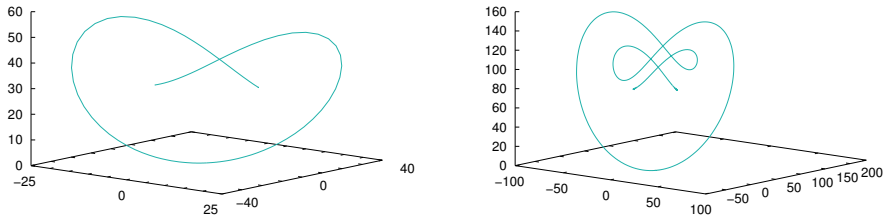

Figure 5.2: Heteroclinic connections givin rise to T-point configurations. See text for details on the parameters used.

In Fig. 5.1 we can see that a section of a solid color corresponds to a constant kneading invariant (we have approximated the Kneading invariant by the 50 first values). By the theorem for varies of parameters in the same color region, one expect that the Lorenz attractor are topologically conjugated while a curve between two solid colors correspond to a bifurcation. That is, different color sections actually prove that the kneading invariant are different and hence this Lorenz attractors are not topologically equivalents.

Another important result we can get from the Kneading invariant and the map shown in Fig. 5.1 is the detection of bifurcations within the Lorenz attractor. In particular we can look for parameters having one-dimensional heteroclinic connexions between the origin and $C_{1,2}$. These global configurations are referred as T-points [13], [1], [3]. The first T-point is given by $\sigma = 10.1673, \beta = 8/3$ and $\rho = 30.868$, for which each branch of the unstable manifold of the origin coincides with the branch of the stable manifold of C_1 and C_2 as shown in the left Fig. 5.2. This parameters are related with the loss of transversality of the strong foliation as it was shown in [1] and [3]. A second T-point which occurs for $\sigma = 11.8279, \beta = 8/3$ and $\rho = 85.0292$, that is, for parameters located at the center of the main spiral structure detected in Fig. 5.1. The corresponding heteroclinic orbit is displayed in Fig. 5.2 right.

As a final conclusion, the Kneading plot shows us that there are several topological Lorenz attractors and provides an approximation of the parameters for which the topological changes (i.e. the bifurcations) occur.

Future work

In this work, we have focused on the study of different dynamical aspects of the Lorenz system. We end this work referring to some aspects that have been left for the future due to lack of time.

A good topic to go in depth would be the verification through numerical integration of the foliation transversality. One can use a grid of points between the stationary points C_1 and C_2 and integrate the flow and the variational equations for each point. Firstly, one can check the transversality of the foliation for the classical parameters $\sigma = 10$, $\beta = 8/3$ and $\rho = 28$. From here one can verify the same condition for different parameters of ρ and stablish some hypothesis over the parameter space related with the foliation transversality.

The computer assisted proof done by W. Tucker showed me a set of methodologies to study dynamical systems. The usage of an algorithm that guarantees the accuracy of the results, suggest to study other dynamical systems through a computer assisted proof.

The Kneading theory allow us to study the parameter space of the Lorenz system and detect bifurcations within the Lorenz attractor. It could be interesting to analyse these T-points and the bifurcations structure of the parameter space.

Appendix A

Numerical integration

Taking the Lorenz equations

$$\begin{cases} \dot{x} = \sigma(y - x) \\ \dot{y} = \rho x - y - xz \\ \dot{z} = -\beta z + xy \end{cases}$$

with a given initial conditions, we want to find a function $x : [a, b] \longrightarrow \mathbb{R}^m$ that gives an approximation of the solution of the Cauchy problem.
Using Picard's (existence and uniqueness) theorem we can claim that the solution exists and is unique. So we can use Taylor's method to approximate it. In the following we briefly summarize this method and we give details on how it can be applied to the Lorenz equations. We closely follow the paper by A. Jorba [8].

A.1 Taylor method

Suppose that we know $x(t), y(t), z(t)$ for some $t \in \mathbb{R}$, we want to compute $x(t+h), y(t+h), z(t+h)$, where h is an appropriate step, using Taylor series of order N.

$$x(t+h) = x(t) + x'(t)h + x''(t)\frac{h^2}{2} + \cdots + x^{(N)}\frac{h^N}{N!} = \sum_{k=0}^{N} x^{(k)}\frac{h^k}{k!}$$

Considering $x^{[k]}(t) = \frac{1}{k!}x^{(k)}$, where $x^{[0]}(t) = x(t)$, then the Taylor series can be written as

$$x(t+h) = \sum_{k=0}^{N} x^{[k]}h^k$$

In this case, x is a three component vector: x, y, z.

A.2 Automatic differentiation

Let's see how to calculate $x^{[k]}(t)$ for $k \geq 1$:

$$
\begin{aligned}
x^{[1]}(t) &= x'(t) = \sigma(y^{[0]} - x^{[0]}) \\
x^{[2]}(t) &= \tfrac{1}{2}x''(t) = \tfrac{\sigma}{2}(y'(t) - x'(t)) = \tfrac{\sigma}{2}(y^{[1]} - x^{[1]}) \\
x^{[3]}(t) &= \tfrac{1}{3!}x^{(3)}(t) = \tfrac{\sigma}{3!}(y''(t) - x''(t)) = \tfrac{\sigma}{3}(y^{[2]}(t) - x^{[2]}(t)) \\
&\vdots \\
x^{[k]}(t) &= \tfrac{1}{k!}x^{(k)}(t) = \tfrac{\sigma}{k!}(y^{(k-1)} - x^{(k-1)}) = \tfrac{\sigma}{k}(y^{[k-1]} - x^{[k-1]})
\end{aligned}
$$

Then we can find $x^{[k]}(t)$ recursively from: $x^{[0]}(t), \cdots, x^{[k-1]}(t)$ i $y^{[0]}(t), \cdots, y^{[k-1]}(t)$. In the same way, we will compute the automatic differentiation of $y(t)$ and $z(t)$.

$$
\begin{cases}
x^{[k]}(t) = \frac{\sigma}{k}(y^{[k-1]} - x^{[k-1]}) \\
y^{[k]}(t) = \frac{1}{k}(\rho x^{[k-1]}(t) - y^{[k-1]}(t) - (xz)^{[k-1]}(t)) \\
z^{[k]}(t) = \frac{1}{k}(-\beta z^{[k-1]}(t) + (xy)^{[k-1]}(t))
\end{cases}
$$

So it's only left to know how to calculate $(xz)^{[k-1]}(t))$:

Proposition A.1.

$$(x \cdot y)^{[k]}(t) = \sum_{j=0}^{k} x^{[j]} \cdot y^{[k-j]}.$$

For a detailed proof, see [8].

A.3 Step size control and degree

As we have seen, to apply Taylor's method, we have to find the appropriate value h_m for every step of Taylor.

$$x_{m+1} = x_m(t_m + h_m) = \sum_{k=0}^{N} x_m^{[k]} \cdot h_m^k.$$

We describe how to find h_m so that the error is small (below a prefixed value ε). So we want to take a h_m value small enough such that

$$||x_m(t_{m+1}) - x_{m+1}|| \leq \varepsilon,$$

where $t_{m+1} = t_m + h_m$, $x_{m+1} = \sum_{k=0}^{N} x_m^{[k]}(t_m)h_m^k$ and ε the tolerance. Following [8] this can be achieved by computing

$$\rho_m^{(j)} = \left(\frac{\varepsilon}{||x_m^{[j]}||_\infty}\right)^{\frac{1}{j}}, \qquad 1 \leq j \leq p,$$

and then using the estimate $h_m = \min\{\rho_m^{(N-1)}, \rho_m^{(N)}\}$ for the step-size.

We have implemented the Taylor method adapted to the Lorenz system following the previous guidelines. All the figures showing quantitative data of this work have been computed using our implementation.

Appendix B

Lyapunov function

While studying the character of stationary points, usually a Lyapunov functions is needed to prove Lyapunov stability. In the case of Lorenz equations, a Lyapunov function is used to proof that the origin is globally attractor for $0 < \rho < 1$, see section 2.1. In this appendix we briefly review the main ideas of Lyapunov stability.

Definition B.1. Let $F : \mathbb{R}^n \longrightarrow \mathbb{R}^n$ be a flux. $V : U \subset \mathbb{R}^n \longrightarrow \mathbb{R}$ is a **Lyapunov function** for F centered at $p \in U$ (where U is an open neighbourhood of p) if

1. $V(x) > 0$ for $x \in U \backslash \{p\}$,
2. $V(p) = 0$,
3. $\frac{d}{dt}V(x(t)) = \langle \nabla V(x), F(x) \rangle \leq 0$.

Note that $F(p) = p$ is forced by this definition.
If in the third condition, $\frac{d}{dt}V(x(t))$ is strictly negative, we call V a **strictly Lyapunov function**.

The existence of a Lyapunov function of a vector field, allow us to study the stability of a stationary point of F. Because of the interest of this study, only the globally asymptotically stability of Lyapunov will be explained.

Globally asymptotically stable
If the Lyapunov-candidate-function V is globally positive definite, radially unbounded and the time derivative of the Lyapunov-candidate-function is globally negative definite:

$$\dot{V}(x) < 0 \qquad \forall x \in \mathbb{R}^n \backslash \{0\},$$

then the equilibrium is proven to be globally asymptotically stable.

Bibliography

[1] R. Barrio, A. Shilnikov and L. Shilnikov, *Kneadings, symbolic dynamics and paintinc Lorenz chaos. A tutorial*, International Journal of Bifurcations and Chaos, (2012)

[2] H. Broer and F. Takens, *Dynamical Systems and Chaos*, Applied Mathematical Science **172**. Springer-Verlag, (2011)

[3] Jennifer L. Creaser, B. Krauskopf and H. M. Osinga, *Finding first foliation tangencies in the Lorenz system*, Preprint (2017).

[4] R. L. Devaney, *An Introduction to Chaotic Dynamical Systems*, Addison-Wesley Publishing Company, Inc. (1989)

[5] J. Guckenheimer and P. Holmes, *Nonlinear Oscillations, Dynamical Systems, and Bifurcations of Vector Fields*, Applied Mathematical Science **42**. Springer-Verlag, (1983)

[6] J. Guckenheimer and R. F. Williams, *Structural stability of Lorenz attractors*, Publication mathématiques de l'IHES, **50** (1979), 59-72

[7] A. Haro, M. Canadell, J. Figueras, A. Luque and J. Mondelo, *The Parameterization method for Invariant manifolds*, Springer-Verlag, (2016)

[8] A. Jorba and M. Zou, *A software package for the numerical integration of ODEs by means of high-order Taylor methods*, Experimental Mathematics, **14**, 1 (2005), 99-117

[9] E. D. Lorenz, *Deterministic nonperiodic flow*, Journal of the Atmospheric Science, **20** (1963), 130-141

[10] S. Luzzatto, I. Melbourne and F. Paccaut, *The Lorenz attractor is mixing*, Communications in Mathematical Physics, (2005), 393-401

[11] M.J. McGuinness, *The fractal dimension of the Lorenz attractor*, Physics Letters, **99A** (1983), 5-9.

[12] D. Rand, *The topological classification of Lorenz attractors*, Mathematical Proceedings of the Cambridge Philosophical Society, **83** (1978), 451-460

[13] C. Sparrow, *The Lorenz equations: bifurcations, chaos and strange attractors*, Applied Mathematical Science **41**. Springer-Verlag, 1982

[14] W. Tucker, *A rigorous ODE solver and Smale's 14th problem*, Foundations of Computational Mathematics, (2002), 53-117

[15] D. Viswanath, The fractal property of the Lorenz attractor. Physica D, 190 (2004), 115-128.

[16] R. Williams, *The structure of Lorenz attractors*, Publication mathématiques de l'IHES, **50** (1979), 321-347